

## The scaling characteristics of remotely-sensed variables for sparsely-vegetated heterogeneous landscapes

M. Susan Moran<sup>a,\*</sup>, Karen S. Humes<sup>b</sup>, Paul J. Pinter Jr.<sup>a</sup>

<sup>a</sup>USDA-ARS US Water Conservation Laboratory, 4331 E. Broadway Road, Phoenix, AZ 85719, USA

<sup>b</sup>USDA-ARS Hydrology Laboratory, Building 007, BARC-West, Beltsville, MD 20705, USA

---

### Abstract

With increasing interest in airborne and satellite-based sensors for mapping regional and global energy balance, there is a need to determine the uncertainty involved in aggregating remotely-sensed variables [surface temperature ( $T_k$ ) and reflectance ( $\rho$ )] and surface energy fluxes [sensible ( $H$ ) and latent ( $\lambda E$ ) heat flux] over large areas. This uncertainty is directly related to two factors: (1) the non-linearity of the relation between the sensor signal and  $T_k$ ,  $\rho$ ,  $H$  or  $\lambda E$ ; and (2) the heterogeneity of the site. In this study, we compiled several remotely-sensed data sets acquired at different locations within a semi-arid rangeland in Arizona, at a variety of spatial and temporal resolutions. These data sets provided the range of data heterogeneities necessary for an extensive analysis of data aggregation. The general technique to evaluate uncertainty was to compare remotely-sensed variables and energy balance components calculated in two ways: first, calculated at the pixel resolution and averaged to the coarser resolution; and second, calculated directly at the coarse resolution by aggregating the fine-resolution data to the coarse scale. Results showed that the error in the aggregation of  $T_k$  and  $\rho$  was negligible for a wide range of conditions. However, the error in aggregation of  $H$  and  $\lambda E$  was highly influenced by the heterogeneity of the site. Errors in  $H$  larger than 50% were possible under certain conditions. The conditions associated with the largest aggregation errors in  $H$  were:

- sites which are composed of a mix of stable and unstable conditions;
- sites which have considerable variations in aerodynamic roughness, especially for highly unstable conditions where the difference between surface and air temperature is large; and
- sites which are characterized by patch vegetation, where the pixel resolution is less than or nearly-equal to the diameter of the vegetation 'element' (in most cases, the diameter of the dominant vegetation type or vegetation patch).

Thus, knowledge of the surface heterogeneity is essential for minimizing error in aggregation of  $H$

---

\* Corresponding author. Tel: +1 602 670 6481; fax: +1 602 607 6493.

and  $\lambda E$ . Two schemes are presented for quantifying surface heterogeneity as a first step in data aggregation. These results emphasized the need for caution in aggregation of energy balance components over heterogeneous landscapes with sparse or mixed vegetation types. © 1997 Elsevier Science B.V.

---

## 1. Introduction

Remote sensing using airborne and satellite-based sensors is useful for estimating surface energy fluxes such as sensible ( $H$ ) and latent ( $\lambda E$ ) heat flux over large areas. There are many algorithms and simulation models designed for this purpose. Most of these approaches utilize remote measurements of surface temperature and reflectance to compute the components of the energy balance equation [ $H$ , net radiation ( $R_n$ ) and soil heat flux ( $G$ )] and estimate  $\lambda E$  as a residual of the energy balance (see background section). Nearly all approaches require some supplementary meteorological and/or surface information.

The extent of surface information required draws a distinction between those approaches that can be applied at a local scale and those limited to regional application (Moran and Jackson, 1991). Most local scale methods rely on site-specific measurements of aerodynamic and atmospheric conditions and apply only to an area over which the ground-based measurements can be extrapolated. Regional scale methods generally rely on meteorological data from existing weather stations, extrapolated in space and interpolated in time to correspond to the location and moment of the remotely-sensed measurement.

There is interest in aggregating remotely sensed variables (and surface energy fluxes derived from these variables) from local to regional scales. This interest is due to the desire to (1) apply local-scale approaches with regional-scale data and (2) validate results of regional-scale methods by comparison with results of local-scale methods. These goals require investigation of methods for both aggregation of remotely-sensed variables (particularly, radiometric temperature,  $T_r$ ) and aggregation of energy balance components ( $R_n$ ,  $G$ ,  $H$  and  $\lambda E$ ).

This study addresses the issues of aggregation related specifically to heterogeneous landscapes at local and regional scales. Based on several sets of spectral images with spatial resolutions ranging from 0.3 m to 120 m, we studied the effects of aggregation by computing remotely sensed variables and energy balance components in two ways. First, the variable (e.g.  $H$ ) was computed from the radiance at the pixel resolution (e.g. 120 m) and these values were averaged to obtain a value of  $H$  at a coarser resolution (e.g. 1 km). Second, pixel-resolution values of radiance were averaged to the coarser scale and then a value of  $H$  was computed. The difference between these two computations of  $H$  revealed the error due to non-linearities in the relation between surface radiance and  $H$ .

The presentation is organized into sections, with the first section presenting the basic energy balance theory that is the foundation for most local- and regional-scale models and defining the relation between kinetic, radiometric and aerodynamic temperatures. The

second section discusses the issues directly related to aggregation of data for heterogeneous landscapes and suggests a method for quantifying site heterogeneity. The third section describes the study site, the sensor characteristics, and the methods for acquisition of data for this research. Finally, aggregation results are presented for a variety of homogeneous and heterogeneous sites at various scales.

## 2. Background

### 2.1. Energy balance theory

In general, estimation of energy flux using remotely-sensed data is based on the solution of the one-dimensional surface energy balance equation, expressed as

$$R_n = G + H + \lambda E, \quad (1)$$

where  $R_n$ ,  $G$ ,  $H$  and  $\lambda E$  are in units of  $\text{W m}^{-2}$ , and  $G$ ,  $H$  and  $\lambda E$  are positive when directed away from the surface.  $\lambda E$  is a function of evaporation rate,  $E$  ( $\text{kg s}^{-1} \text{m}^{-2}$ ), and heat of vaporization,  $L$  ( $\text{J kg}^{-1}$ ), but is typically found as a residual in Eq. (1).

$R_n$  can also be defined as the sum of the incoming and outgoing radiant flux densities, i.e.

$$R_n = (1 - \alpha)R_{\text{SI}} + R_{\text{LI}} - R_{\text{LJ}}, \quad (2)$$

where  $\alpha$  is the hemispherical albedo, the subscripts S and L signify shortwave radiation (0.15 to  $\approx 4 \mu\text{m}$ ) and longwave radiation ( $>4 \mu\text{m}$ ) and the arrows indicate the flux direction ( $\downarrow$ : incoming;  $\uparrow$ : outgoing).  $R_n$  is generally estimated in one of two ways: (1) it can be measured using net radiometers and extrapolated over the region of interest; or (2) it can be computed using remotely-sensed measurements to estimate  $\alpha$  and  $R_{\text{L}\uparrow}$ , and ground-based instrumentation to measure the incoming terms (Jackson, 1984; Brest and Goward, 1987).

The  $G$  term is dependent upon the gradient of temperature,  $T$  ( $^{\circ}\text{K}$ ), with soil depth,  $z$  (m),

$$G = -K(dT/dz), \quad (3)$$

where  $K$  is thermal conductivity ( $\text{W m}^{-1} \text{K}^{-1}$ ). Results from empirical studies have shown that the daytime ratio of  $G/R_n$  is related to, among other factors, the amount of vegetation present (de Bruin and Holtslag, 1982). Thus, an approximation of  $G$  can be achieved by assuming that it is a fraction of  $R_n$ , dependent upon spectral estimates of surface vegetation cover (Moran et al., 1990; Kustas and Daughtry, 1990; Clothier et al., 1986). In some cases, such as for full-cover vegetation,  $G$  is assumed to be negligible and eliminated from the solution of Eq. (1).

The sensible heat flux density,  $H$ , is commonly expressed as a function of the difference between the aerodynamic temperature ( $T_o$ ) and air temperature ( $T_a$ ),

$$H = C_v(T_o - T_a)/r_a, \quad (4)$$

where  $C_v$  the volumetric heat capacity of air ( $\text{J } ^{\circ}\text{C}^{-1} \text{m}^{-3}$ ), and  $r_a$  is the aerodynamic resistance to heat transport ( $\text{s m}^{-1}$ ). This resistance for neutral conditions (where

$T_o = T_a$ ) is

$$r_a = \{\ln[(z-d)/z_o]\}^2/k^2 U, \quad (5)$$

where  $z_o$  and  $d$  are roughness length and zero-plane displacement (m), respectively,  $U$  is wind speed ( $\text{m s}^{-1}$ ),  $z$  is the height (m) above the surface where  $U$  is measured, and  $k$  ( $= 0.41$ ) is von Karman's constant (Brutsaert, 1982). In most cases, adjustments are made to Eq. (5) to account for non-neutral conditions ( $T_o \neq T_a$ ) (e.g. Marht and Ek, 1984; Brutsaert, 1982; Lang et al., 1983).

## 2.2. Temperature definitions

It is important at this point in the discussion to make a distinction between  $T_o$ , kinetic temperature ( $T_k$ ) and radiometric temperature ( $T_r$ ). Aerodynamic temperature is recognized to be the temperature at the virtual source/sink height for sensible heat exchange. The kinetic (absolute) temperature is a measure of the average kinetic energy of atomic and molecular units in motion within bodies above absolute zero. The radiometric (apparent) temperature is an estimate of the kinetic temperature, generally evaluated from a measurement of radiation emitted from the surface using an infrared sensor (Jackson, 1988).

The emittance ( $M_r$ ,  $\text{W m}^{-2}$ ) measured by a radiometer close to a surface (i.e. neglecting atmospheric effects in measurements acquired with an aircraft or satellite-based sensor) in a finite spectral band is related to the emittance of the surface ( $M_k$ ,  $\text{W m}^{-2}$ ) with the expression

$$M_r = \epsilon M_k + (1 - \epsilon) M_s \quad (6)$$

where  $\epsilon$  is the emissivity of the surface in the finite spectral band (assumed constant over the band) and  $M_s$  ( $\text{W m}^{-2}$ ) is the incoming atmospheric emittance in the spectral band. These emittances are theoretically quantified by integrating the product of the sensor response function and the Planck function over the finite spectral band of the sensor. By integrating the Planck function over the wavelength interval 0 to  $\infty$ , one obtains the Stefan–Boltzmann law ( $M = \epsilon \sigma T^4$ , where  $\sigma$  is the Stefan–Boltzmann constant:  $5.674 \times 10^{-8} \text{ W m}^{-2} \text{ K}^{-4}$ ). For simplicity here, the Stefan–Boltzmann expression is substituted for each term in Eq. (6) to obtain the expression

$$\sigma T_r^4 = \epsilon \sigma T_k^4 + (1 - \epsilon) B^* \quad (7)$$

In the above expression, the term  $B^*$  includes the incoming sky radiation in the spectral band 0 to  $\infty$  and a factor related to the ratio of incoming sky radiation in the finite spectral band to incoming sky radiation in the spectral band 0 to  $\infty$  (after Fuchs and Tanner, 1966). The emissivity term is eliminated from the left hand side of the equation because the infrared sensor is calibrated with a blackbody with emissivity close to 1. Thus, the kinetic temperature is derived from the radiometric temperature by inversion of Eq. (7).

Many studies show that  $T_k$  and  $T_o$  correspond well for the case of full-cover vegetation (e.g. Huband and Monteith, 1986). However, for partially-vegetated sites,  $T_k$  and  $T_o$  have been found to differ by as much as  $5^\circ\text{C}$  (Choudhury et al., 1986). From here on,  $T_o$  will refer to the temperature obtained by inverting Eq. (4),  $T_r$  will refer to the temperature

measured with an infrared sensor (as described above), and  $T_k$  will refer to  $T_r$  with a correction for  $\epsilon$  as described by Eq. (7).  $\epsilon$  is the ratio of emittance of a given surface to the emittance of an ideal blackbody at the same wavelength and temperature.

### 3. Issues related to aggregation

Aggregation is simple when all relations between surface radiance and surface reflectance and temperature are linear and when relations between surface reflectance and temperature and surface energy fluxes are linear. Aggregation of remotely-sensed variables such as  $\alpha$  and  $T_k$  becomes more complicated when their relations with radiance are non-linear due to emissivity, sensor optics and/or atmospheric conditions. The errors associated with aggregation of surface fluxes ( $R_n$ ,  $G$ ,  $H$  and  $\lambda E$ ) estimated with remotely-sensed variables is a function of the error associated with aggregation of remotely-sensed data and the non-linear relations between remotely-sensed inputs to the computation of surface fluxes.

This study will focus on the issues associated with aggregation of  $T_k$  and  $H$ . For the following reasons, aggregation of  $\alpha$ ,  $R_n$ ,  $G$  and  $\lambda E$  will not be addressed here:

- $\alpha$ : There is a great deal of published evidence that the relation between radiance and reflectance (and  $\alpha$ ) is linear for most sensors and most atmospheric conditions (Hall et al., 1992; Humes and Sorooshian, 1994; Holm et al., 1989; Moran et al., 1994b). We obtained similar results for the surface and atmospheric conditions in this study, so presentation of such results was considered redundant.

- $R_n$ : It is apparent from Eq. (2) that the shortwave component of  $R_n$  is a linear function of the surface albedo, which has a linear relation with radiance. The longwave components of  $R_n$  ( $R_{L\downarrow}$  and  $R_{L\uparrow}$ ) are related to air and surface temperatures, respectively, using the well-known Stefan–Boltzmann equation (Brutsaert, 1975a). Thus, the magnitude of error in  $R_{L\downarrow}$  would be directly related to that associated with aggregation of  $T_k$ . Since aggregation of  $T_k$  will be addressed in this study, it was deemed unnecessary to repeat the analysis for  $R_{L\downarrow}$ . Actually, the variables that are associated with most of the error in aggregation of  $R_n$  are the incoming terms ( $R_{S\downarrow}$  and  $R_{L\downarrow}$ ) which are generally estimated with ground-based instrumentation and are thus unrelated to remotely-sensed data.

- $G$ : There is evidence that the relation of  $G/R_n$  is linearly or near-linearly related to a spectral vegetation index computed from the ratio of the near-IR and red reflectances (Kustas and Daughtry, 1990; Clothier et al., 1986; Moran et al., 1990). Again, since previously-published studies reported a linear relation between reflectance and radiance, there is little chance for error in the aggregation of values of  $G$  from local to regional scales.

- $\lambda E$ : Since  $\lambda E$  is computed as a residual in the energy balance equation (Eq. (1)), the sum of the errors associated with aggregation of  $R_n$ ,  $G$  and  $H$  would equal the error in  $\lambda E$ . And since we are assuming negligible error in aggregation of  $R_n$  and  $G$ , the results of our study of aggregation of  $H$  are directly applicable to estimates of  $\lambda E$ .

In the following subsections, we will address the issues related to aggregation of  $T_k$  and  $H$  and the relation of aggregation error with surface heterogeneity.

### 3.1. Aggregation of temperature data

The relation between radiance measured by a satellite sensor and values of surface temperature is not necessarily linear. For example, the relation between  $T_r$  and spectral radiance ( $L$ ) is given for Landsat Thematic Mapper (TM) as

$$T_r = K_2 / [\ln(K_1/L + 1)], \quad (8)$$

where  $K_2$  (K) and  $K_1$  ( $\text{mW cm}^{-2} \text{s}^{-1} \mu\text{m}^{-1}$ ) were determined for Landsat4 and Landsat5 TM by Markham and Barker (1986). This equation is a close approximation of the integration of the Planck function over the spectral bands of the TM sensor. Because temperature is a slightly non-linear function of observed radiance, the aerially-integrated temperatures derived from radiance observed with sensors of low- and high-resolution over the same area may be slightly different.

Furthermore, the radiometers provide only an estimate of the radiometric temperature with no correction for surface emissivity. As shown in Eq. (7), an emissivity less than unity decreased the apparent temperature, whereas the reflection of incoming sky radiation increased it by a different amount (Fuchs and Tanner, 1966). Thus, the data collected using ground- or satellite-based sensors must be corrected for the surface emissivity. For a series of natural surfaces within a savanna environment, Van de Griend and Owe (1993) found that  $\epsilon$  could be estimated as

$$\epsilon = 1.0094 + 0.042(\ln(\text{NDVI})), \quad (9)$$

where NDVI is the Normalized Difference Vegetation Index  $[(\rho_{\text{NIR}} - \rho_{\text{red}})/(\rho_{\text{NIR}} + \rho_{\text{red}})]$  and  $\rho_{\text{NIR}}$  and  $\rho_{\text{red}}$  are the near-IR and red reflectances, relatively. The NDVI was derived to be sensitive to changes in vegetation cover (Richardson and Wiegand, 1977); thus, it appears that the relation between  $\epsilon$  and vegetation cover is logarithmic.

### 3.2. Aggregation of sensible heat flux

For relatively homogenous landscapes, Hall et al. (1992, Section 3.2.1) found that the relation between remotely sensed TM data and radiance was sufficiently linear to allow  $H$  values derived with TM-resolution (30 m or 120 m) remotely-sensed data to be averaged to produce low-resolution (1 km) values with little error. However, based on a theoretical evaluation of the eddy diffusion formulation of  $H$  (Eq. (4)), they predicted a breakdown in scale invariance for heterogeneous landscapes (their Section 2.4.1). Scale invariance may not hold for heterogeneous landscapes (such as semi-arid rangeland) for three reasons. First, substantial variations in vegetation type, height and cover associated with heterogeneous landscapes result in large variations in resistance to heat transfer (Monteith, 1973, 1981). There is also evidence that resistance is dependent upon the magnitude of the difference between the soil and foliage temperature (Kustas et al., 1989). In semiarid rangelands, the difference between soil and vegetation temperature can be as large as  $40^\circ\text{C}$  (Humes et al., 1994b). Thus, one would expect a greater error in the averaged values of  $H$  and  $\lambda E$  for a heterogeneous site than for a homogeneous landscape.

Second, heterogeneous landscapes would likely include surfaces with both stable ( $T_o < T_a$ ) and unstable ( $T_o > T_a$ ) conditions. Thus, the neutral equation for resistance must be

corrected for effects of stability. In most formulations, the stability correction results in a non-linear relation between  $T_o$  and  $r_a$  and, consequently, would result in a non-linear relation between fluxes aggregated from fine-resolution data and those computed with coarse-resolution data.

Third, there is a non-linear relation between  $T_k$  and  $T_o$  over a range of vegetation densities. That is, the difference between  $T_o$  and  $T_k$  is small for fully-vegetated surfaces (or sites with little difference between soil and vegetation temperatures) and increases rapidly with increasing heterogeneity of the surface (when the difference between soil and vegetation temperatures is large). For a surface only partially covered by vegetation (where  $T_k$  is a composite of the soil and vegetation temperatures), Kustas et al. (1990) reported that the resistance to heat transfer was significantly influenced by rapid changes in the soil surface temperature. Thus, observed values of  $H$  several meters above the surface changed relatively little compared with changes in  $T_k - T_a$  (Kustas et al., 1989). Consequently, for partially-vegetated surfaces, it is necessary to incorporate an additional or 'excess' resistance to sensible heat transfer.

Several studies have addressed the computation of an excess resistance term based on the fact that momentum transfer (based on pressure and viscous forces) is more efficient than transfer of scalar quantities, such as  $H$ , which are transferred by viscous forces only (Brutsaert, 1975b). This results in additional resistance to heat transfer that can be expressed in the resistance equation by including different roughness lengths for momentum (subscript  $m$ ) and heat (subscript  $h$ ), where

$$r_a' = \{[\ln((z-d)/z_{om}) + \ln(z_{om}/z_{oh}) - \psi_h][\ln((z-d)/z_{om}) - \psi_m]\}/k^2U \quad (10)$$

and  $z_{om}$  and  $z_{oh}$  are the roughness length for momentum and scalar roughness for heat, respectively, and  $\psi_h$  and  $\psi_m$  are the stability corrections for heat and momentum (summarized by Beljaars and Holtslag, 1991). A  $kB^{-1}$  factor [defined  $kB^{-1} = \ln(z_{om}/z_{oh})$ ] was included in the resistance computation, resulting in a non-linear relation between  $(T_k - T_a)$  and  $H$ . Thus, it is possible to rewrite Eq. (4) as

$$H = C_v(T_k - T_a)/r_a' \quad (11)$$

In application, Kustas et al. (1989) suggested that  $kB^{-1}$  could be computed as a function of wind speed ( $U$ ) and  $(T_k - T_a)$  and proposed that

$$kB^{-1} = s_{kb}U(T_k - T_a), \quad (12)$$

where  $s_{kb}$  is site-specific and was computed as 0.17 for Owens Valley rangeland and 0.13 for Walnut Gulch rangeland (Kustas et al., 1994b).

There is substantial evidence supporting the importance of accounting for the difference between  $T_o$  and  $T_k$  in Eq. (4) (e.g. Choudhury et al., 1986). Though inclusion of the  $kB^{-1}$  factor in the resistance term is only one of several approaches that have been proposed to account for the difference between  $T_o$  and  $T_k$  (others include Chehbouni et al., 1994; Vidal and Perrier, 1990; Norman et al., 1994; Shuttleworth and Wallace, 1985; Kustas, 1990; Moran et al., 1993; Prevot et al., 1993), it was adopted for use in this study due to extensive studies that have proven its application for semi-arid rangeland (Moran et al., 1994c; Humes et al., 1994a; Kustas et al., 1994b,c; Stewart et al., 1994).

### 3.3. Relation of surface heterogeneity to aggregation

The issues identified above for aggregation of  $T_k$  and  $H$  are inextricably linked to the heterogeneity of the site. For example, the sensor calibration presented in Eq. (8) is nearly-linear for a large range of  $T_r$  values, resulting in little error in aggregation for homogeneous sites with a low range of  $T_r$  values. The same is true for the error associated with emissivity, where the logarithmic relation between  $\epsilon$  and NDVI will produce little scaling error for uniformly-vegetated sites with a low range of NDVI values. And the scaling errors associated with the stability corrections in Eq. (10) will produce the greatest scaling errors for heterogeneous sites with an equal distribution of stable and unstable conditions. Thus, it is important to quantify the heterogeneity of the site before attempting aggregation of the remotely-sensed variables or energy balance components.

The importance of quantifying heterogeneity is matched by its difficulty. The variability of remotely-sensed variables and energy balance components for a site is influenced by surface-related factors such as vegetation type/cover and soil moisture, and other factors such as time of day, time of year and spatial resolution. This complexity leads to some misconceptions about site heterogeneity. For example, at one time of day at one site, the variability in  $T_r$  for a sparsely-vegetated rangeland site would probably be less during the 'dry' season than during the 'wet' season when vegetation and soil moisture are highly variable. However, an early-morning measurement during the wet season would have less variability than a mid-day measurement during the dry season (due to differential heating of vegetated and bare surfaces). Furthermore, a fine-resolution image during the dry season would likely show more variability than a coarse-resolution image during the monsoon season. Thus, it is erroneous to make the assumption that all sites will be heterogeneous during the wet season and homogeneous during the dry season.

In this study, we used two methods to quantify the heterogeneity of a site. The first was simply a comparison of the shapes, magnitudes and ranges of histograms formed from image data. The second method utilized a scattergram of the NDVI versus surface-air temperature ( $T_k - T_a$ ) from the spectral image. The significance of the latter requires some theoretical background which will be provided here, though readers are encouraged to refer to previously-published works (Price, 1990; Gillies and Carlson, 1994; Nemani and Running, 1989; Moran et al., 1994a).

A scattergram of the spectral vegetation index (e.g. NDVI or soil-adjusted vegetation index (SAVI), Huete, 1988) vs.  $T_k - T_a$  generally results in a trapezoidal shape that is indicative of the variation in vegetation cover and evapotranspiration (e.g. Fig. 1). Carlson et al. (1990) associated the scatter with differences in root-zone moisture availability (5–100 cm), soil surface moisture (0–2 cm) and fraction of vegetation cover. The shape of the scatter is thus related to the heterogeneity of the site. Boundaries can be drawn encompassing the maximum-possible variability in the vegetation index and  $T_k - T_a$ , allowing determination of the absolute heterogeneity of the site defined by meteorological conditions. Moran et al. (1994a) proposed a theoretical basis for computing the maximum and minimum possible surface temperatures for a range of vegetation cover from 0 to 100% using a variation of the Penman-Monteith

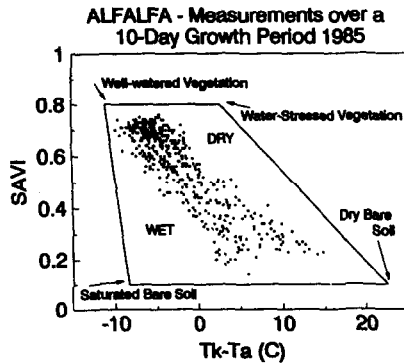


Fig. 1. An example of a scattergram of values of  $(T_k - T_a)$  and SAVI measured in well-watered and water-deficit alfalfa treatment plots with differing vegetation cover ranging from near-zero to 100% cover (From Moran et al., 1994a). The solid lines represent the trapezoidal shape that would result from the relation between the SAVI and computed with  $(T_k - T_a)$  the Penman-Monteith equation for complete vegetation cover (SAVI = 0.8) and bare soil (SAVI = 0.1).

equation,

$$(T_k - T_a) = [r_a'(R_n - G)/C_v][\gamma(1 + r_c/r_a')/\{\Delta + \gamma(1 + r_c/r_a')\}] - [VPD/\{\Delta + \gamma(1 + r_c/r_a')\}], \quad (13)$$

where  $r_c$  the canopy resistance ( $s\ m^{-1}$ ) to vapor transport,  $\gamma$  the psychrometric constant ( $kPa\ ^\circ C^{-1}$ ),  $\Delta$  the slope of the saturated vapor pressure-temperature relation ( $kPa\ ^\circ C^{-1}$ ), and VPD the vapor pressure deficit of the air ( $kPa$ ). This work resulted in the derivation of a Vegetation-Index/Temperature (VIT) Trapezoid that encompassed the maximum possible variability in the vegetation index and values of  $(T_k - T_a)$  for one site on one date (Fig. 1).

The VIT Trapezoid theory defines  $T_k - T_a$  for four extreme situations by changing the  $r_c$  term in Eq. (13):

1. Full-cover, well-watered vegetation, where  $r_c$  is the canopy resistance at potential evapotranspiration (assumed to be  $5\ s\ m^{-1}$ );
2. Full-cover vegetation with no available water ( $\lambda E = 0$ ), where  $r_c$  is the canopy resistance associated with nearly complete stomatal closure (assumed to be  $1000\ s\ m^{-1}$ );
3. Saturated bare soil, where  $r_c = 0$  (the case of a free water surface); and
4. Dry bare soil, where  $r_c = \infty$  (analogous to complete stomatal closure).

The left edge of the trapezoid was related to conditions of potential evapotranspiration and the right edge was related to conditions in which  $\lambda E = 0$ . Thus, the location of the image data within the trapezoid provides information about the variability of  $H$  and  $\lambda E$ , in addition to the basic information on variability of the vegetation index and  $T_k - T_a$ . The VIT trapezoid will be used in subsequent sections to illustrate the heterogeneity of the study sites.

### 3.4. Summary of issues

In order to test any schemes for aggregation of  $T_r$  and  $H$ , variability in the following points must be considered:

1. sensor calibration;
2. surface emissivity;
3. site aerodynamic stability;
4.  $z_0$  between sites; and
5.  $z_{om}$  and  $z_{oh}$  at each point.

Furthermore, these issues are interrelated and effects of each are dependent upon the variability of other features. Thus, it is equally important to consider the heterogeneity of the site in any aggregation scheme. Using an extensive set of remotely-sensed and meteorological data acquired in a semiarid rangeland in Arizona during the dry and wet season, a first attempt will be made to define the sensitivity of linear aggregation schemes to these points.

### 4. Data sets and methods of analysis

An experiment was conducted at the Walnut Gulch Experimental Watershed (WGEW) near Tombstone, AZ, to acquire the meteorological and remote sensing data necessary to evaluate the scaling characteristics of heterogeneous landscapes. These data were acquired as part of larger study (Monsoon '90) focusing on the general utility of remote sensing to provide a practical means for monitoring some of the important factors controlling land surface processes (Kustas et al., 1991). The experimental sites were located in an area comprising the upper 100 km<sup>2</sup> of the Walnut Gulch drainage basin, from about 1300–1800 m above mean sea level (MSL). In this region, precipitation ranges from 250–300 mm year<sup>-1</sup>, with 2/3 of the rainfall occurring during the summer 'monsoon season' in July and August. For this study, data were obtained during the dry season in June while most vegetation was still dormant, and during the monsoon season in late July and early August, when the vegetation was at peak greenness and soil moisture was highly variable in time and space due to recent precipitation events (Schmugge et al., 1994).

Most of the analysis was limited to eight sites within the watershed, termed METFLUX stations (herein referred to as MF1 to MF8), containing instrumentation for measuring both general meteorological conditions and estimating the surface energy balance (Kustas et al., 1994a). The METFLUX sites were located along two parallel transects crossing the two dominant vegetation types (brush and grasses) and the transition from one to the other (Fig. 2). Two of the eight METFLUX sites contained considerably more micrometeorological instrumentation than the others: MF1 (located in the Lucky Hills subwatershed) was located in a relatively flat, brush-dominated ecosystem and MF5 (Kendall subwatershed) was in a hilly, grass-dominated subwatershed.

Some analysis was conducted for a site just southeast of WGEW that included a distinct riparian zone, characterized by lush perennial vegetation. The riparian zone presented a linear feature in high contrast with surrounding brush and grassland vegetation, resulting in very heterogeneous conditions.

#### 4.1. Data sets

Data from four sensors mounted on four different platforms were used for this analysis. The platforms, sensor characteristics, locations of ground targets, and dates of data acquisition are summarized in Table 1. A more detailed account of data acquisition methods and site descriptions follows.

**Yoke-based radiometers:** Radiometers were mounted on backpack-type devices (yokes) to be carried by operators at two sites (Lucky Hills and Kendall) to characterize by sparse shrubs and grass, respectively. At both sites, a large ground target was delimited over which surface temperature and reflectance were measured from a height of 2 m above the ground surface, using yoke-based radiometers and a calibrated reference reflectance panel (Jackson et al., 1987). Data were acquired at 1 m increments along transects through the target, covering the entire target in less than 15 min (this technique was similar to that described by Slater et al., 1987). The Lucky Hills target was approximately 120 by 120 m in size, typified by relatively flat topography and primarily shrub vegetation of  $\approx 0.6$  m height covering 20% of the soil surface. The Kendall target was much larger, 480 by 120 m, located in a hilly, grass-dominated site, stretching from the top of one hill eastward to the top of another. Yoke-based spectral data were processed to produce reflectance and temperature for individual samples (0.3 m resolution) on days of year (DOYs) 156 and 252 (to correspond with TM data) at 10.30 h at Lucky Hills and Kendall.

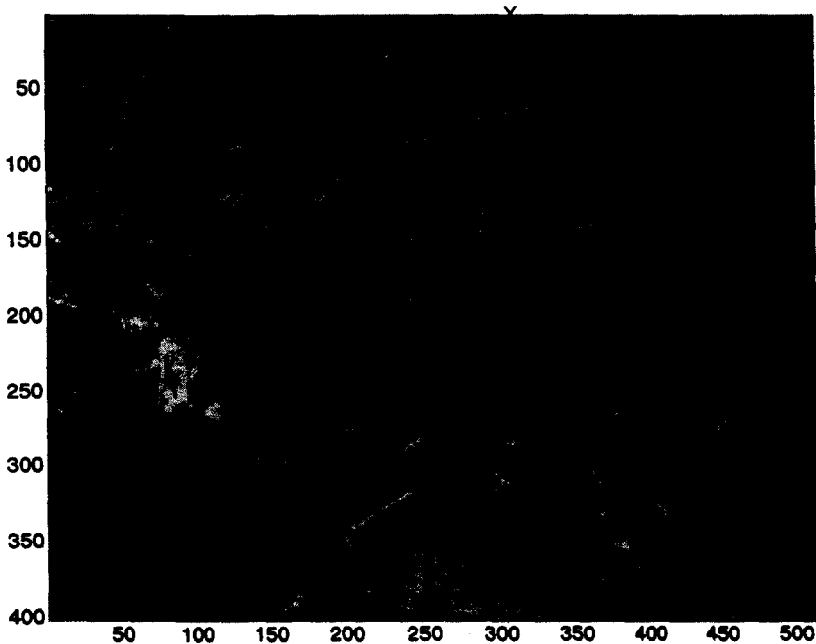


Fig. 2. Landsat TM image covering WGEW and the area immediately surrounding. The solid lines delimit the boundaries of the WGEW and RIP targets. The flight paths of the Cessna and C130 aircraft intercepted the locations of the eight METFLUX sites (X).

**Thermal Scanner:** Thermal infrared data were acquired over WGEW with an Infra-metrics 600 thermal imaging radiometer during the Monsoon '90 Experiment. The scanner was flown in a single engine Cessna at altitudes ranging from 0.09 km to 3.35 km above ground level (AGL) on several days from DOY 209 to DOY 222. A subset of these data were selected coinciding with clear-sky conditions and a variety of surface conditions. Thermal data were selected for Kendall and Lucky Hills on three dates at 0.09 km AGL: DOY 209 at 10.12 h, DOY 209 at 14.40 h and DOY 221 at 07.30 h. Thermal data acquired at higher altitudes, 0.92 km and 3.35 km AGL, were selected for Lucky Hills on DOY 222 at 14.11 h and Kendall on DOY 209 at 14.51 h, respectively. In all cases, a window of size 380 by 480 pixels was extracted surrounding the designated METFLUX site. Thus, at a flight altitude of 0.09 km AGL, the window covered an area of 76 by 96 m and at 3.35 km AGL the window covered 2.3 by 2.9 km.

**NS001:** The C-130 aircraft with the NS001 sensor flew at an altitude of 2 km AGL along transects intersecting the locations of the 8 METFLUX sites. Windows of size approximately 2.3 by 2.9 km were extracted for areas surrounding each of the eight METFLUX sites. Though the NS001 sensor provides data in eight spectral bands, at this time only the thermal data were available. We limited our analysis to data collected during a mid-day flight on DOY 221 with cloudfree conditions.

**Landsat TM:** Landsat-5 TM data were acquired on DOY 156 (dry season) and 252 (post-monsoon season) covering an area 180 by 180 km, encompassing WGEW. Analysis was conducted for two adjacent areas of size 10 by 3 km within the scene. One area

Table 1

General description of instruments deployed during the Monsoon' 90 Experiment

Platform	Instrument	No. of bands	Wave-length range	Targets	Flight dates (day of year 1990)
Yoke	Exotech Radiometer, IFOV: 15°	4	0.50–0.89 $\mu\text{m}$	Kendall: 0.48 $\times$ 0.12 km	156252
	Everest IRT, IFOV: 15°; Footprint: 0.3 m	1	8–13 $\mu\text{m}$	Lucky Hills: 0.12 $\times$ 0.12 km	
Cessna	Thermal Infrared Scanner: IFOV 2.4 mrad; Footprint: 0.2 m at 0.09 km AGL; 1.7 m at 0.92 km AGL; 6.0 m at 3.35 km AGL	1	8–12 $\mu\text{m}$	Kendall and Lucky Hills: 380 pixels by 480 lines	209221 at 0.09 km AGL; 222 at 0.92 km; 209 at 3.35 km
C-130	NS001 Thematic Mapper Simulator, IFOV: 2.5 mrad; Footprint: 6.0 m	8	0.46–12.3 $\mu\text{m}$	All eight METFLUX Sites: approximate size 380 pixels by 480 lines	221
Landsat-5	Thematic Mapper (TM); Footprint: 30 m Reflected and 120 m Emitted	7	0.45–12.5 $\mu\text{m}$	Two targets: WGEW and RIP (Riparian site) 10 km by 3 km each	156252

covered most of WGEW and another covered an area just southeast of WGEW that included very diverse terrain and some pixels with distinctive riparian vegetation (this area will be referred to as RIP to distinguish it from WGEW). Prior to any tests of aggregation, the reflected data (TM1-TM4) were averaged from 30 m resolution to 120 m resolution to provide reflected and emitted data at the same resolution.

We emphasize that these data sets were selected for analysis because they covered a wide range of conditions due to differences in spatial resolution, time of acquisition, and site characteristics. The study presented here is not meant to be an evaluation of the effects of *spatial resolution and other data-specific characteristics* on aggregation, but rather an evaluation of the effects of *surface heterogeneity* on aggregation. The differences in the spatial resolution, timing, and location of these data sets resulted in differences in the heterogeneity of the surface temperatures and reflectances that were necessary for an extensive analysis of data aggregation. Though we realize that most interest in aggregation is at the regional and global scales, the aggregation of our finest resolution data (less than plant diameter) provided the opportunity for insight into the uncertainty of aggregation at coarser scales (e.g. sites characterized by distinctive patch vegetation).

#### 4.2. Methods of analysis

All analyses had the same general form. Values of  $T_r$  and  $H$  were each computed in two ways:

*Surface temperature:* First,  $T_r$  was computed from radiance at the pixel resolution (e.g. 120 m for TM) and corrected for emissivity (using Eqs. (7) and (9)), where  $B^*$  was assumed to be zero and NDVI was computed for each pixel), and these values were averaged to obtain a value of  $T_k$  at a coarser resolution (e.g. 1 km for TM). Second, pixel-resolution values of radiance were averaged to the coarser scale (e.g. 1 km for TM) and then a value of  $T_r$  was computed and corrected for emissivity (based on an average NDVI value in Eq. (9)) to estimate  $T_k$ . All tests in which visible and near-IR data were available (yoke and TM), temperatures were corrected for emissivity using Eqs. (7) and (9). In all other tests, we assumed that  $\epsilon = 1.0$  for all temperatures.

*Sensible heat flux:* First,  $H$  was computed from  $T_k$  at the pixel resolution (Eqs. (10)–(12)) and these values were averaged to obtain a value at the coarser resolution. Second, pixel-resolution values of  $T_k$  were averaged to the coarser scale, and then a value of  $H$  was computed using Eqs. (10)–(12) based on average values of  $T_k$ . All tests were conducted using resistance equations that included the  $kB^{-1}$  factor, using  $s_{kB} = 0.17$ . In all cases, corrections were made for stability conditions; that is, different equations were used for stable and unstable conditions, according to Beljaars and Holtslag (1991). Meteorologic inputs ( $z$ ,  $U$  and  $T_a$ ) were taken from a local station for the time of the spectral measurements, and values of  $z_0$  and  $d$  for these sites were computed by Kustas et al. (1994a).

For all data sets except TM, the data were aggregated from pixel-resolution to a single point covering the entire extracted window. The TM data were aggregated from 120 m to 1 km resolution over the window covering a 10 by 3 km area. Thus, the aggregation of TM data resulted in 30 (that is,  $10 \times 3$ ) pixels, and the aggregation for all other data sets resulted in a single value for each.

## 5. Results: site variability

To investigate the variability of the vegetation index and  $T_r - T_a$  for the finest (yoke) and coarsest (TM) resolutions, the VIT Trapezoid was computed for WGEW based on on-site meteorological data for DOY 156 and 252. As described previously, the left edge of the trapezoid is related to conditions of potential evapotranspiration and the right edge is related to conditions in which  $\lambda E = 0$ . The yoke-based data illustrated the variability at sub-element scale (0.3 m resolution < plant diameter) and the TM data illustrate variability of mixed pixels (120 m resolution  $\gg$  plant diameter). For DOY 156 (dry season), the yoke and TM data were clustered in the lower right corner of the VIT Trapezoid, indicating low vegetation cover and dry conditions (Fig. 3(a)). The variability of the yoke-based NDVI and  $T_k - T_a$  data was much larger than that of the TM data, even though the area of coverage was much smaller. For the TM data, the variability of the WGEW site was lower than that of the RIP site which encompassed a distinct riparian zone.

For DOY 252, the yoke and TM data were shifted toward the left edge of the trapezoid, indicating higher  $\lambda E$  values associated with the wet season (Fig. 3(b)). The general variability of NDVI and  $T_k - T_a$  was much greater than for DOY 156 at both resolutions. The variability of the yoke data at Lucky Hills (MF1) was greater than the same data for Kendall (MF5). Similar to results for DOY 156, the variability of the yoke data was greater than that of the TM data, and the variability of the TM data for the RIP site was greater than that for WGEW.

When only thermal data were available, we were unable to use the NDVI vs.  $T_k - T_a$  scattergram to evaluate site heterogeneity. Instead, we evaluated the relative site heterogeneity by comparing the histograms of  $T_r - T_a$  from images acquired at different times of day and locations. Since thermal scanner images were acquired at several locations, altitudes, times of day, and times of season, it was possible to investigate the influence of these factors on the variability of  $T_r - T_a$ :

- Time of Day: The range of  $T_r - T_a$  values increased with time of day at both Lucky Hills and Kendall (Fig. 4(A) and Table 2). This was due to the differential thermal inertia and evapotranspiration of vegetation and soil, and it generally results in greater absolute variability near noon. However, since one of the issues to be addressed in aggregation of  $H$  is the non-linear relation between  $T_k - T_a$  and atmospheric stability, we must also consider the mix of unstable and stable conditions. The early morning measurements tend to have a greater mix of stable and unstable conditions; later readings tended toward uniformly unstable conditions.
- Time of year: Images acquired on DOY 209 (early-monsoon) and DOY 221 (mid-monsoon) for the same site and time of day were used to investigate the influence of seasonal vegetation differences (Fig. 4(B) and Table 2). Though the range of  $T_r - T_a$  values decreased slightly with the increase in soil moisture and vegetation cover associated with the monsoon season, the most distinctive feature of these data was the shift of the histogram peak by nearly 5°C, associated with more actively transpiring vegetation component on DOY 221.
- Vegetation type/cover: The variability associated with vegetation type and cover

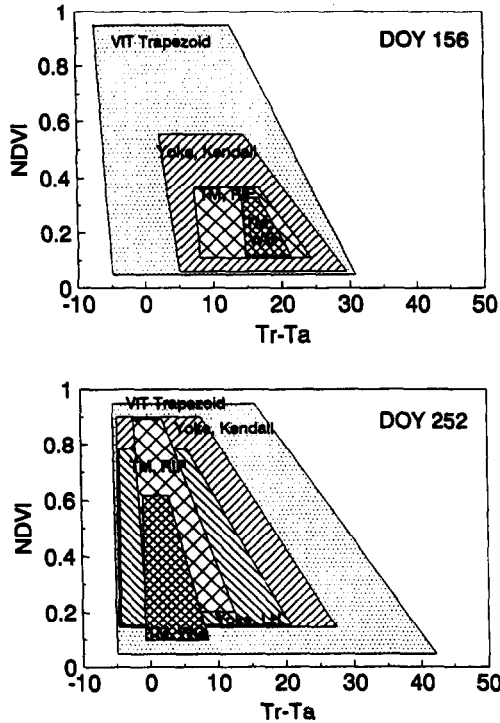


Fig. 3. An illustration of the variability of the yoke-based (0.3 m resolution) and TM spectral data (120 m resolution) for WGEW and RIP on DOYs 156 and 252.

was illustrated by comparison of  $T_r - T_a$  values for the Kendall and Lucky Hills sites on the same day and time, with the same spatial resolution (Fig. 4(C) and Table 2). Kendall was characterized by a uniform distribution of grass; whereas, Lucky Hills was characterized by scattered shrubs and bare soil. Consequently, the histogram of data from Kendall formed a unimodal distribution skewed toward higher temperatures, and the histogram of Lucky Hills' data tended toward a bimodal shape with peaks associated with the shrubs and bare soil (Humes et al., 1994b).

- **Spatial resolution:** Thermal data acquired near the same time-of-day at two spatial resolutions (0.2 m and 6.0 m) with a field of view centered on Kendall were compared (Fig. 4(D) and Table 2). As expected, the coarser resolution data had less variability than the finer resolution data; the range of  $T_r - T_a$  values decreased from 27°C (at 0.2 m resolution) to 13°C (at 6.0 m resolution). This was the case even though the coarser-resolution image covered a ground surface area that was larger and more variable than the smaller area covered by the finer-resolution image. Thus, it is apparent that at these scales the highest variability in  $T_r - T_a$  is associated with the finer resolutions.

It should be noted that this analysis was conducted without correction of the thermal

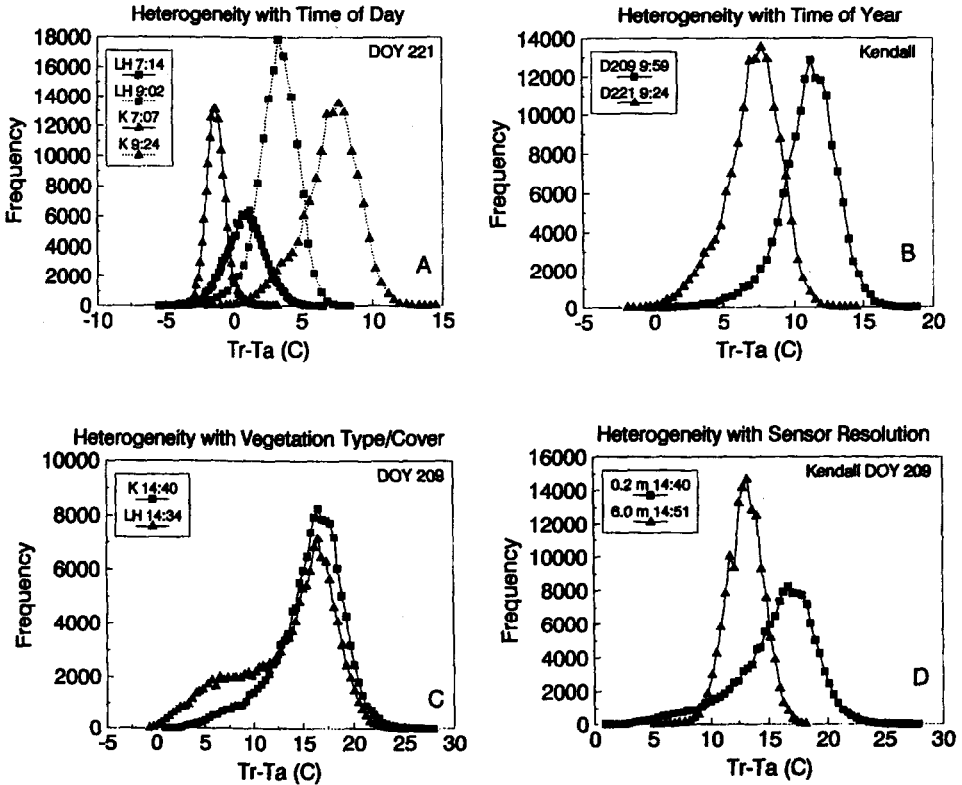


Fig. 4. Comparisons of histograms of thermal scanner data to illustrate the variability of  $T_r - T_a$  values due to influences of (A) time of day; (B) time of year; (C) vegetation type/cover; and (D) sensor spatial resolution.

data for atmospheric attenuation. As precipitable water increases, ground temperatures detected by airborne and satellite sensors tend to converge (Kiang, 1982). Consequently, the overall effect of the atmosphere is to reduce the thermal image contrast (Byrnes and Schott, 1986). This would affect the results presented in Fig. 3 and Fig. 4, where data acquired on different days, at different sites, or at different altitudes were directly compared. This effect could partially explain the decrease in variability of the satellite data relative to that of the yoke-based data (Fig. 3) and the decrease in variability with sensor resolution (Fig. 4(D)). The atmospheric influence would have less effect on the following analysis in which aggregation techniques are applied to single images and the within-image variation is presented.

## 6. Results: aggregation

In previous sections, we identified several sources of non-linearity in the relation between radiance and  $T_r$  (due to sensor calibration), between  $T_r$  and  $T_k$  (due to emissivity),

Table 2

Summary of statistics associated with histograms of thermal scanner data (acquired with the Cessna aircraft flying at 0.09 km to 3.35 km above ground level) presented in Fig. 4. ‘Skew’ is the 3rd moment about the mean, where a larger absolute value represents a more pronounced skew and a negative number indicates a skew to the right. ‘SD’ is one standard deviation from the mean, where  $n = 143\,112$  in all cases

Figure	Time of day (h)	Day of year	Location	Spatial resolution	Range of $T_r - T_a$ values °C	Skew	SD
4A	07.14	221	L. Hills	0.2 m	10.5	0.06	1.44
4A	09.02	221	L. Hills	0.2 m	13.9	-0.73	1.48
4A	07.07	221	Kendall	0.2 m	7.6	-0.45	0.72
4A	09.24	221	Kendall	0.2 m	16.4	-0.57	2.00
4B	09.59	209	Kendall	0.2 m	21.3	-0.75	2.07
4B	09.24	221	Kendall	0.2 m	16.4	-0.57	2.00
4C	14.40	209	Kendall	0.2 m	27.0	-0.85	3.44
4C	14.34	209	L. Hills	0.2 m	25.7	-0.72	4.73
4D	14.40	209	Kendall	0.2 m	27.0	-0.85	3.44
4D	14.51	209	Kendall	6.0 m	13.0	-0.23	1.58

and between  $T_k - T_a$  and  $H$  (due to stability corrections of  $r_a$  and variability in surface roughness,  $z_o$ ). Here, we used data from the yoke-based radiometers, aircraft-based thermal scanner and NS001, and satellite-based TM to investigate the effects of these non-linearities on aggregation of  $T_k$  and  $H$ . As described previously, the general technique to evaluate the error was to compare  $T_k$  and  $H$  values calculated in two ways: first, calculated at the pixel resolution and averaged to the coarser resolution; and second, calculated directly at the coarse resolution by aggregating the fine-resolution data to the coarse scale and then computing  $T_k$  or  $H$ .

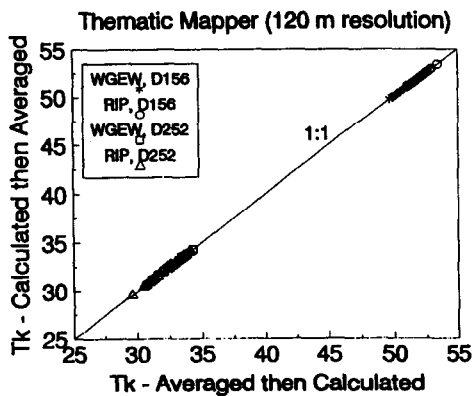


Fig. 5. An investigation of the effect of emissivity and sensor calibration on aggregation of surface temperature estimates from Landsat TM data. Kinetic temperatures ( $T_k$ ) were calculated using eqns (7)–(9) with TM6 radiance and TM estimates of NDVI for WGEW and RIP on DOYs 156 and 252.

### 6.1. Variability in aggregated values of $T_k$ due to sensor calibration and surface emissivity

The relation between  $T_r$  and radiance measured by the TM sensor is nearly linear over a large range of  $T_r$  values and resulted in aggregation errors less than 0.05°C for temperature ranges of 30°C for prairie vegetation in Kansas (Humes and Sorooshian, 1994) during FIFE, the First ISLSCP Field Experiment (Sellers et al., 1988). Similar results were found here for the TM data acquired for WGEW on DOYs 156 and 252. Since this error again proved to be both small and quantifiable (using Eq. (8)), it will not receive further discussion.

The error in aggregation of  $T_k$  associated with the logarithmic relation between emissivity and NDVI (Eq. (9)) was investigated using the TM and yoke-based data sets. The error in aggregation associated with the emissivity correction (and including the non-linearity in the sensor calibration) was minor for the TM-resolution data over the range of surface temperatures associated with two sites and two dates (Fig. 5). The average difference in  $T_k$  values using the two aggregation schemes was less than 0.1°C. The error in aggregation associated with the emissivity correction was also minor for the yoke-based data at a much finer resolution (0.3 m) than TM with a larger range of  $T_r$  values. In this case, the differences in  $T_r$  using the two aggregation schemes were less than 0.04°C.

These results lead to the conclusion that error associated with aggregation of  $T_k$  due to emissivity differences was negligible for both fine and coarse resolutions for relatively homogeneous sites. The error increased slightly (though it was still less than 0.1°C) for heterogeneous sites, such as RIP on DOY 252.

### 6.2. Variability in aggregated values of $H$ due to the stability correction of $r_a$

In the following tests, we assumed that  $z_o$  was constant at both the pre- and post-aggregation scale. In this way, we could investigate the variability in  $H$  associated with variability in the stability correction of  $r_a'$  and variability in  $kB^{-1}$ . By comparing results at different sites and different resolutions, we tested the magnitude of error associated with magnitude of  $z_o$ , stability correction, and emissivity.

At fine resolution (0.3 m for yoke-based and low-altitude thermal scanner data), error in aggregation of  $H$  associated with the stability correction of  $r_a$  could be large, depending on surface conditions. For the yoke-based data, errors as large as 12 W m<sup>-2</sup> were found for highly variable sites such as Lucky Hills during the wet season (Fig. 6). Error was smaller for sites with less variability, such as the Kendall grassland during both the wet and dry seasons. It is notable that the site conditions during data acquisition of yoke-based data (at 10.30 h) were dominated by unstable conditions.

In contrast, the low-altitude thermal scanner data (with footprint of 0.3 m) was acquired during morning, mid-day and afternoon, resulting in data sets acquired with stable conditions, unstable conditions, and a mix of the two. The error in aggregation of  $H$  was small (>10 W m<sup>-2</sup>) for DOY 209 when site variability was low during the early-monsoon season (Fig. 7). Error was larger (nearly 20 W m<sup>-2</sup>) for DOY 221 during the early morning, when the site was characterized by a mix of stable and unstable conditions.

For moderate resolution (6.0 m) NS001 data, error in aggregation associated with the stability correction was small (< 6 W m<sup>-2</sup>) for all METFLUX sites. As with the yoke-

based data, the data were acquired during mid-day when unstable conditions dominated the site ( $T_k - T_a > 0$ ) for most pixels. Results were similar for the coarse resolution (120 m) TM data. The error associated with aggregation of data acquired during the dry season was negligible for both the WGEW and RIP sites. For data acquired during the wet season (DOY 252) at WGEW and RIP, there was greater error though it was still small ( $< 5 \text{ W m}^{-2}$ ).

In conclusion, error associated with aggregation of  $H$  when  $z_0$  was held constant during pre-aggregation and post-aggregation computations was larger for sites with a mixture of stable and unstable conditions (e.g. morning measurements with thermal scanner and yoke-based measurements at Lucky Hills, DOY 252) than for sites dominated by unstable conditions (mid-day measurements in most cases). The error appeared to decrease with increasingly coarser resolution. The differences in  $r_s'$  associated with differences in stability were especially large when the site was composed of an even mixture of stable and unstable conditions at the pixel scale, due to the high non-linearity of the relation between  $H$  and  $T_k - T_a$  (e.g. Fig. 8). Thus, there were large errors observed for morning measurements at WGEW, when this condition was most common.

### 6.3. Variability in aggregated values of $H$ due to variability in $z_0$

To test the sensitivity of aggregation of  $H$  values to the non-linearity in the relation between  $T_k - T_a$  and  $H$  due to varying surface roughness conditions, we assumed that  $z_0$  was one value for shrub-dominated sites (0.04 m) and another for grass-dominated sites (0.01 m) at the pre-aggregation scale ( $z_0$  values computed by Kustas et al., 1994a), and  $z_0$  was either 0.04 m or 0.01 m for the post-aggregation scale. Thus, there were three outputs from the aggregation: (1)  $H$  computed with a variable  $z_0$  value related to shrub or grass cover; (2)  $H$  computed with a constant  $z_0 = 0.04 \text{ m}$ ; and (3)  $H$  computed with a constant  $z_0 = 0.01 \text{ m}$ . This test was conducted by combining the data extracted for each METFLUX

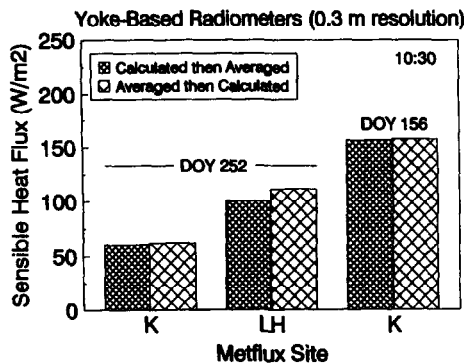


Fig. 6. An investigation of the effect of the  $r_s'$  stability correction on aggregation of sensible heat flux ( $H$ ) using yoke-based data. Values of  $H$  were calculated using Eqs. (7), (9)–(12), and yoke-based measurements of  $T_s$  and NDVI for Kendall (K) and Lucky Hills (LH) on DOYs 156 and 252 at 10:30.  $z_0$  was assumed to be constant at both scales, though different for each site.

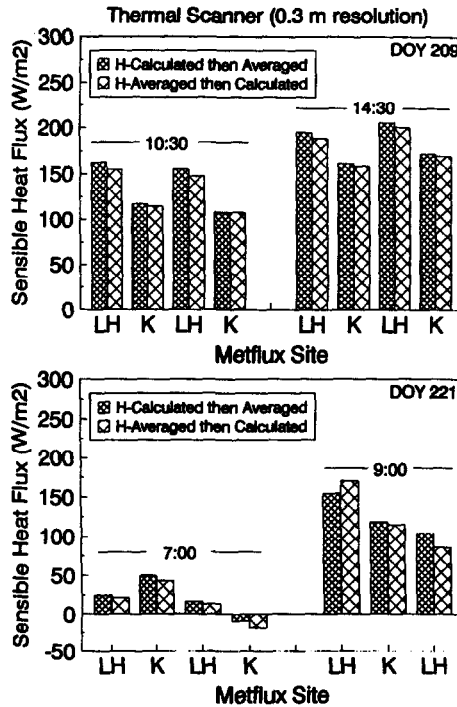


Fig. 7. An investigation of the effect of the  $r_s'$  stability correction on aggregation of sensible heat flux ( $H$ ) using thermal scanner data. Values of  $H$  were calculated using Eqs. (10)–(12) and thermal scanner measurements of  $T_k$  for Kendall (K) and Lucky Hills (LH) on DOY 209 and DOY 221.  $z_0$  was assumed to be constant at both scales, though different for each site.

site from the thermal scanner and NS001 images. In this way, we could investigate the variability in  $H$  associated with all the above-mentioned surface variability *and* variability in  $z_0$ .

For thermal scanner data with fine resolution (0.3 m), there were large differences (nearly  $50 \text{ W m}^{-2}$ ) between values of  $H$  aggregated with differing  $z_0$  values, especially in mid-afternoon (Fig. 9). There was negligible error ( $< 5 \text{ W m}^{-2}$ ) associated with measurements in the early morning when values of  $H$  were small ( $\approx 35 \text{ W m}^{-2}$ ). For NS001 data with moderate resolution (6.0 m), the error in aggregation of  $H$  was smaller ( $< 25 \text{ W m}^{-2}$ ) (Fig. 10) than for the higher-resolution thermal scanner data.

We concluded that substantial errors in  $H$  could be expected (at all spatial resolutions) in aggregation of sites with significantly different values of  $z_0$ . This was especially true for measurements at midday when the range and magnitude of  $T_k - T_a$  values were large. The differences in  $H$  associated with differences in  $z_0$  could be especially large when values of  $T_k - T_a$  were large (e.g. Fig. 8). Thus, errors were smaller for morning measurements than for measurements in the afternoon.

It is apparent from the simulated data in Fig. 8 that the inclusion of a variable  $kB^{-1}$  term in Eq. (10) resulted in a non-linear relation between  $T_k - T_a$  and  $H$  in Eq. (11). Though the

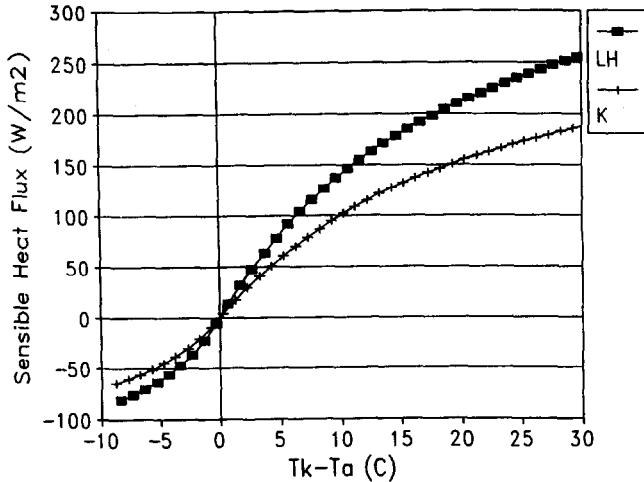


Fig. 8. Comparison of  $H$  values computed for a continuum of  $(T_k - T_a)$  values DOY 252 at 10.30 h at Kendall ( $z_0 = 0.01$  m) and Lucky Hills ( $z_0 = 0.04$  m) for stable and unstable conditions. These data illustrate the non-linearity of the relation between  $(T_k - T_a)$  and  $H$ , and the differences in the relation due to variations in roughness.

use of a constant  $kB^{-1}$  term would minimize the errors in aggregation of  $H$  for heterogeneous sites, it would substantially increase the absolute error in estimation of  $H$  (Moran et al., 1994c).

Since  $\lambda E$  is computed as a residual in most remote sensing models utilizing Eq. (1) and since we assumed here that there would be little error associated with aggregation of  $R_n$  and  $G$ , the error associated with aggregation of  $H$  is directly related to the error in  $\lambda E$ . In some cases (e.g. Fig. 9), the error in  $H$  increased with its magnitude. Since  $\lambda E$  decreases in

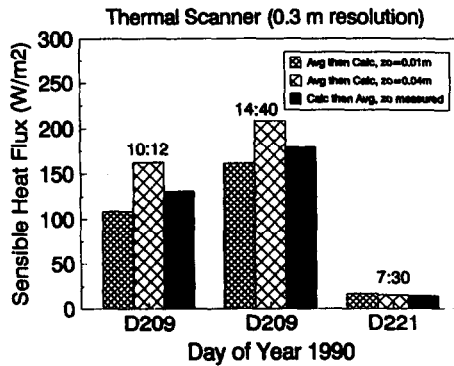


Fig. 9. An investigation of the effect of stability corrections of  $r_a'$  and site-specific differences in  $z_0$  on estimates of sensible heat flux ( $H$ ) using thermal scanner data. Values of  $H$  were calculated using eqns (10)–(12) and thermal scanner measurements of  $T_k$  for a combined data set of Lucky Hills and Kendall on DOY 209 at 10.12 h, DOY 209 at 14.40 h, and DOY 221 at 7.30 h.  $z_0$  was assumed to be 0.01 m at Kendall and 0.04 m at Lucky Hills for the bars labeled 'z<sub>0</sub> measured'.

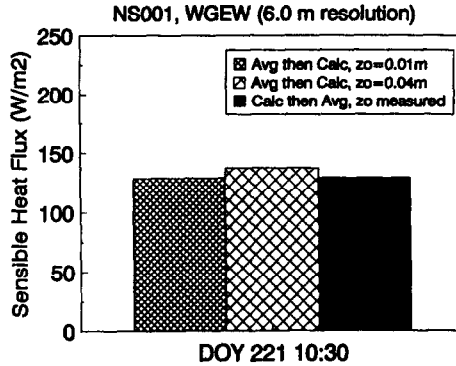


Fig. 10. An investigation of the effect of stability corrections of  $r_s'$  and site-specific differences in  $z_0$  on estimates of sensible heat flux ( $H$ ) using NS001 data. Values of  $H$  were calculated using eqns (10)–(12) and NS001 measurements of  $T_k$  for a combined set of data from all MF sites on DOY 221 at 10:30.  $z_0$  was assumed to be 0.01 m at MF3–MF7 and 0.04 m at MF1, MF2 and MF8 for the bar labeled ' $z_0$  measured'.

magnitude as  $H$  increases, the resultant error in  $\lambda E$  relative to its magnitude would be quite large.

## 7. Conclusions

Previous studies have shown that simple linear aggregation of surface reflectance, albedo and spectral vegetation indices results in near-negligible error for most conditions (Humes and Sorooshian, 1994; Hall et al., 1992). In this study, we confirmed that non-linearities in the TM thermal sensor calibration and conversion from  $T_r$  to  $T_k$  (accounting for emissivity) were also negligible over most ranges of  $T_r$ . However, we found that aggregation of surface energy balance components was more complicated and, under many conditions, the error was substantial.

This study emphasized the need to account for site heterogeneity in selection of a scheme for aggregation of surface energy balance components. This is particularly true for sparsely-vegetated sites, such as the Walnut Gulch semi-arid rangeland. However, the quantification of site heterogeneity is not an easy task since it can be related not only to vegetation cover but also to time of day, time of year and sensor spatial resolution. Thus, it is important to understand the sources of non-linearity in the computation of  $H$  and  $\lambda E$  in order to understand the errors associated with aggregation.

Caution should be used in aggregation of energy balance components over heterogeneous landscapes with sparse or mixed vegetation types. Substantial error can be obtained with the following conditions:

- Sites which are composed of a mix of stable and unstable conditions;
- Sites which have considerable variations in aerodynamic roughness, especially for highly unstable conditions where  $T_k - T_a$  is large; and
- Sites which are characterized by patch vegetation, where the pixel resolution is less

than or nearly-equal to the diameter of the vegetation 'element' (in most cases, the diameter of the dominant vegetation type or vegetation patch).

Future work should address two issues. First, this analysis addressed only scale issues related to surface heterogeneity. It did not address feedbacks and integrating effects of the atmosphere (Brutsaert, 1986; Jacobs and de Bruin, 1992) that could decrease the potential for error in aggregation that was indirectly illustrated in Fig. 8. Second, results from this analysis showed that there was substantial error in aggregation of  $H$  for sites with differences in surface roughnesses. These results were obtained with the aggregation of sites where roughness varied by only 0.03 m. The aggregation error for sites with greater variation in roughness lengths, such as mixtures of grassland and forest, could be many times larger than that presented here.

### Acknowledgements

The data reported here were taken from a larger data set acquired with support from the NASA Interdisciplinary Research Program in Earth Sciences (NASA Ref. Num. 1DP-88-086), the NASA Eos Program (NASA Ref. Num. NAG-W2425) and NSF (BSC-8920851). In particular, thanks are due to Bill Kustas and Dave Goodrich, the principal investigators in the Monsoon' 90 Experiment; Tom Clarke, Ghani Chehbouni, Jim Washburne, Gao Xiasong and several other scientists who assisted in field work; and Lynnette Eastman and Rob Perry who were responsible for some aspects of data processing. We also appreciate the cooperation and assistance of personnel at the USDA-ARS Southwest Watershed Research Center, Tucson, and the USDA-ARS Tombstone facility. In this analysis, we solicited technical input from several colleagues including Bill Kustas, John Norman, Toby Carlson, Ghani Chehbouni, Alain Vidal, John Stewart, Laurent Prevot and Bernard Seguin.

### References

- Beljaars, A.C.M. and Holtslag, A.A.M., 1991. Flux parameterization over land surfaces for atmospheric models. *J. Appl. Meteorol.*, 30: 327–341.
- Brest, C.L. and Goward, S.N., 1987. Deriving surface albedo measurements from narrow band satellite data. *Int. J. Rem. Sens.*, 8: 351–367.
- Brutsaert, W.H., 1975a. On a derivable formula for long-wave radiation from clear skies. *Water Resour. Res.*, 11: 742–744.
- Brutsaert, W.H., 1975b. Comments on surface roughness parameters and the height of dense vegetation. *J. Meteorol. Soc. Jpn.*, 53: 96–97.
- Brutsaert, W.H., 1982. *Evaporation into the Atmosphere*. D. Reidel, London, 299 pp.
- Brutsaert, W.H., 1986. Catchment-scale evaporation and the atmospheric boundary layer. *Water Res.*, 22: 39S–45S.
- Byrnes, A.E. and Schott, J.R., 1986. Correction of thermal imagery for atmospheric effects using aircraft measurements and atmospheric modeling techniques. *Appl. Optics*, 25: 2563–2570.

- Carlson, T.N., Perry, E.M. and Schmugge, T.J., 1990. Remote estimation of soil moisture availability and fractional vegetation cover for agricultural fields. *Agric. For. Meteorol.*, 52: 45–69.
- Chehbouni, A., Nichols, W.D., Qi, J., Njoku, E.G., Kerr, Y.H. and Cabot, F., 1994. On the use of radiative surface temperature to estimate sensible heat flux over sparse shrubs in Nevada. 6th Int. Coll. on Phys. Measurements and Signatures in Rem. Sensing, 17–21 January, Val d'Isere, pp. 777–784.
- Choudhury, B.J., Reginato, R.J. and Idso, S.B., 1986. An analysis of infrared temperature observations over wheat and calculation of the latent heat flux. *Agric. For. Meteorol.*, 37: 75–88.
- Clothier, B.E., Clawson, K.L., Pinter, Jr., P.J., Moran, M.S., Reginato, R.J. and Jackson, R.D., 1986. Estimation of soil heat flux from net radiation during the growth of alfalfa. *Agric. For. Meteorol.*, 37: 319–329.
- de Bruin, H.A.R. and Holtslag, A.A.M., 1982. A simple parameterization of the surface fluxes of sensible and latent heat during daytime compared with the Penman-Monteith concept. *J. Appl. Meteorol.*, 21: 1610–1621.
- Fuchs, M. and Tanner, C.B., 1966. Infrared thermometry of vegetation. *Agron. J.*, 58: 597–601.
- Gillies, R.R. and Carlson, T.N., 1994. Thermal remote sensing of surface soil water content with partial vegetation cover for incorporation into climate models. *J. Appl. Meteorol.*, 34: 745–756.
- Hall, F.G., Huemmrich, K.F., Goetz, S.J., Sellers, P.J. and Nickeson, J.E., 1992. Satellite remote sensing of surface energy balance: success, failures and unresolved issues in FIFE. *J. Geophys. Res.*, 97: 19061–19089.
- Holm, R.G., Moran, M.S., Jackson, R.D., Slater, P.N., Yuan, B. and Biggar, S.F., 1989. Surface reflectance factor retrieval from Thematic Mapper data. *Rem. Sens. Environ.*, 27: 47–57.
- Huband, N.D.S. and Monteith, J.L., 1986. Radiative surface temperature and energy balance of a wheat canopy. I. Comparison of radiative and aerodynamic canopy temperature. *Boundary Layer Meteorol.*, 36: 1–17.
- Huete, A.R., 1988. A soil-adjusted vegetation index (SAVI). *Remote Sens. Environ.*, 25: 89–105.
- Humes, K.S., Kustas W.P. and Moran, M.S., 1994a. Use of remote sensing and reference site measurements to estimate instantaneous surface energy balance components over a semi-arid rangeland watershed. *Water Res. Res.*, 30: 1363–1373.
- Humes, K.S., Kustas, W.P., Moran, M.S., Nichols, W.D. and Weltz, M.A., 1994b. Variability in emissivity and surface temperature over a sparsely vegetated surface. *Water Resour. Res.*, 30: 1299–1310.
- Humes, K.S. and Sorooshian, S., 1994. Spatial scaling of two land surface variables derived from remotely sensed data. *J. Appl. Meteorol.*, (submitted).
- Jackson, R.D., 1984. Total reflected solar radiation calculated from multi-band sensor data. *Agric. For. Meteorol.*, 33: 163–175.
- Jackson, R.D., 1988. Surface temperature and the surface energy balance. In: W.L. Steffen and O.T. Denmead (Editors). *Flow and Transport in the Natural Environment: Advances and Applications*. Springer-Verlag, NY, pp. 133–153.
- Jackson, R.D., Moran, M.S., Slater, P.N. and Biggar, S.F., 1987. Field calibration of reference reflectance panels. *Rem. Sens. Environ.*, 22: 145–158.
- Jacobs, C.M.J. and de Bruin, H.A.R., 1992. The sensitivity of regional transpiration to land-surface characteristics: significance of feedback. *J. Climate*, 5: 683–698.
- Kiang, R.K., 1982. Atmospheric effects on TM measurements: characterization and comparison with the effects on MSS. *IEEE Tran. Geosci. Rem. Sens.*, GE-20: 365–370.
- Kustas, W.P., 1990. Estimates of evapotranspiration with a one- and two-layer model of heat transfer over partial canopy cover. *J. Appl. Meteorol.*, 29: 704–715.
- Kustas, W.P., Blanford, J.H., Stannard, D.I., Daughtry, C.S.T., Nichols, W.D. and Weltz, M.A., 1994a. Local estimates of the surface energy balance and momentum roughness length using first order and second order turbulent statistics in semi-arid rangelands. *Water Resour. Res.*, 30: 1351–1361.
- Kustas, W.P., Choudhury, B.J., Moran, M.S., Reginato, R.J., Jackson, R.D., Gay, L.W. and Weaver, H.L., 1989. Determination of sensible heat flux over sparse canopy using thermal infrared data. *Agric. For. Meteorol.*, 44: 197–216.
- Kustas, W.P., Choudhury, B.J., Inoue, Y., Pinter, Jr., P.J., Moran, M.S., Jackson, R.D. and Reginato, R.J., 1990. Ground and aircraft infrared observations over a partially-vegetated area. *Int. J. Rem. Sens.*, 11: 409–427.
- Kustas, W.P. and Daughtry, C.S.T., 1990. Estimation of the soil heat flux/net radiation ratio from spectral data. *Agric. For. Meteorol.*, 49: 205–223.

- Kustas, W. P., Goodrich, D.C., Moran, M.S. et al., 1991. An interdisciplinary field study of the energy and water fluxes in the atmosphere-biosphere system over semiarid rangelands: Description and some preliminary results, *Bull. Am. Meteorol. Soc.*, 72: 1683–1706.
- Kustas, W.P., Moran, M.S., Humes, K.S., Stannard, D.I., Pinter, Jr., P.J., Hipps, L.E., Swiatek, E. and Goodrich, D.C., 1994b. Surface energy balance estimates at local and regional scales using optical remote sensing from an aircraft platform and atmospheric data collected over semiarid rangelands, *Water Resour. Res.*, 30: 1241–1259.
- Kustas, W.P., Perry, E.M., Doraiswamy, P.C. and Moran, M.S., 1994c. Using satellite remote sensing to extrapolate evapotranspiration estimates in time and space over a semiarid rangeland basin, *Rem. Sens. Env.*, 49: 275–286.
- Lang, A.R.G., McNaughton, K.G., Fazu, C., Bradley, E.F. and Ohtaki, E., 1983. Inequality of eddy transfer coefficients for vertical transport of sensible and latent heats during advective inversions. *Boundary-Layer Meteorol.*, 25: 25–41.
- Mahrt, L. and Ek, M., 1984. The influence of atmospheric stability on potential evaporation, *J. Climate Appl. Meteorol.*, 23: 222–234.
- Markham, B.L. and Barker, J.L., 1986. Landsat MSS and TM post-calibration dynamic ranges, exoatmospheric reflectances and at-satellite temperatures. EOSAT Landsat Tech. Notes 1:3–8; available from EOSAT, 4300 Forbes Blvd., Lanham, MD 20706.
- Monteith, J.L., 1973. *Principles of Environmental Physics*. Elsevier, NY, 241 pp.
- Monteith, J.L., 1981. Evaporation and surface temperature. *Quart. J. Royal Meteorol. Soc.*, 107: 1–27.
- Moran, M.S., Clarke, T.R., Inoue, Y. and Vidal, A., 1994a. Estimating crop water deficit using the relation between surface-air temperature and spectral vegetation index. *Remote Sens. Environ.*, 49: 246–263.
- Moran, M.S., Clarke, T.R., Kustas, W.P., Wertz, M.A. and Amer, S.A., 1994b. Evaluation of hydrologic parameters in semiarid rangeland using remotely sensed spectral data, *Water Resour. Res.*, 30: 1287–1297.
- Moran, M.S. and Jackson, R.D., 1991. Assessing the spatial distribution of evapotranspiration using remotely sensed inputs. *J. Env. Qual.*, 20: 725–737.
- Moran, M.S., Jackson, R.D., Raymond, L.H., Gay, L.W. and Slater, P.N., 1990. Mapping surface energy balance components by combining Landsat Thematic Mapper and ground-based meteorological data. *Rem. Sens. Environ.*, 30: 77–87.
- Moran, M.S., Kustas, W.P., Vidal, A., Stannard, D.I., Blanford, J.H. and Nichols, W.D., 1994c. Use of ground-based remotely sensed data for surface energy balance evaluation of a semiarid rangeland. *Water Resour. Res.*, 30: 1339–1349.
- Moran, M.S., Wertz, M.A., Vidal, A., Goodrich, D.C. et al., 1993. Evaluating energy balance of semiarid rangeland from combined optical-microwave remote sensing. *IEEE Topical Symp. on Combined Optical-Microwave Earth and Atmosphere Sensing*, 22–25 March, Albuquerque, NM, pp. 82–85.
- Nemani, R.R. and Running, S.W., 1989. Estimation of regional surface resistance to evapotranspiration from NDVI and thermal-IR AVHRR data. *J. Appl. Meteorol.*, 28: 276–284.
- Norman, J.M., Divakarla, M. and Goel, N.S., 1995. Algorithms for extracting information from remote thermal-IR observations of the earth's surface. *Rem. Sens. Env.*, 51: 157–168.
- Prevot, L., Y. Brunet, K.T. Paw, U. and Seguin, B., 1993. Canopy modelling for estimating sensible heat flux from thermal infrared measurements. *Workshop on Thermal Infrared Remote Sensing of the Energy and Water Balance over Vegetation in Conjunction with other Sensors*, 20–23 September 1993, La Londe.
- Price, J.C., 1990. Using spatial context in satellite data to infer regional scale evapotranspiration. *IEEE Trans. Geosci. Rem. Sens.*, 28: 940–948.
- Richardson, A.J. and Wiegand, C.L., 1977. Distinguishing vegetation from soil background information, *Photogramm. Eng. Rem. Sens.*, 43: 1541–1552.
- Schmugge, T.J., Jackson, T.J., Kustas, W.P., Roberts, R., Parry, R., Goodrich, D.C., Amer, S. and Wertz, M.A., 1994. PBMR observations of surface soil moisture in Monsoon '90, *Water Resour. Res.*, 30: 1321–1327.
- Sellers, P.J., Hall, F.G., Asrar, G., Strelbel, D.E. and Murphy, R.E., 1988. The first ISLSCP field experiment (FIFE). *Bull. Am. Meteorol. Soc.*, 69: 22–27.
- Shuttleworth, W.J. and Wallace, J.S., 1985. Evaporation from sparse crops — An energy combination theory. *Q.J.R. Meteorol. Soc.*, 111: 839–855.

- Slater, P.N., Biggar, S.F., Holm, R.G., Jackson, R.D., Mao, Y., Moran, M.S., Palmer, J.M. and Yuan, B., 1987. Reflectance- and radiance-based methods for the in-flight absolute calibration of multispectral sensors. *Rem. Sens. Environ.*, 22: 11–37.
- Stewart, J.B., Kustas, W.P., Humes, E.S., Nichols, W.D., Moran, M.S. and de Bruin, H.A.R., 1994. Sensible heat flux-radiative surface temperature relationship for eight semi-arid areas. *J. Appl. Meteorol.*, 33: 1110–1117.
- Van de Griend, A.A. and Owe, M., 1993. On the relationship between thermal emissivity and the normalized difference vegetation index for natural surfaces. *Int. J. Rem. Sens.*, 14: 1119–1131.
- Vidal, A. and Perrier, A., 1990. Irrigation monitoring by following the water balance from NOAA-AVHRR thermal infrared data. *IEEE Trans. Geosci. Rem. Sens.*, 28: 949–954.